

# Atmospheric Precorrected Differential Absorption Technique to Retrieve Columnar Water Vapor

Daniel Schl pfer,<sup>\*</sup> Christoph C. Borel,<sup>†</sup> Johannes Keller,<sup>‡</sup>  
and Klaus I. Itten<sup>\*</sup>

*Differential absorption techniques are suitable to retrieve the total column water vapor contents from imaging spectroscopy data. A technique called Atmospheric Precorrected Differential Absorption (APDA) is derived directly from simplified radiative transfer equations. It combines a partial atmospheric correction with a differential absorption technique. The atmospheric path radiance term is iteratively corrected during the retrieval of water vapor. This improves the results especially over low background albedos. The error of the method for various ground reflectance spectra is below 7% for most of the spectra. The channel combinations for two test cases are then defined, using a quantitative procedure, which is based on MODTRAN simulations and the image itself. An error analysis indicates that the influence of aerosols and channel calibration is minimal. The APDA technique is then applied to two AVIRIS images acquired in 1991 and 1995. The accuracy of the measured water vapor columns is within a range of  $\pm 5\%$  compared to ground truth radiosonde data. ©Elsevier Science Inc., 1998*

## INTRODUCTION

Water vapor is one of the main forces for weather development. It also is a key absorber of solar radiation. Current operational imaging systems for water vapor detection

use primarily the emission in the thermal infrared at 5.7–7.1  $\mu\text{m}$  (GOES and Meteosat). The disadvantage of these satellite systems is a coarse spatial (horizontal) resolution, ranging from 5 km (Meteosat) to 8 km (GOES) and a limited penetration into the lower atmosphere (e.g., 700 hPa for Meteosat) (Kramer, 1994; Krishna Rao et al., 1990). Other sensors like ATSR, HIRS, or DMSP are sounders with vertical resolutions in the kilometer range but without any imaging capabilities. Conversely, imaging spectroscopy measures the total column water vapor contents at high spatial horizontal resolutions and has therefore the potential of completing atmospheric sounding systems. The sensors of the AVIRIS instrument are capable of acquiring hyperspectral data in 224 channels located in the visible and near-infrared from 0.4  $\mu\text{m}$  to 2.45  $\mu\text{m}$  at 10 nm resolution. The measured radiances depend on the spectral reflectance of the Earth's surface as well as on absorption and scattering in the atmosphere. Measurements of water vapor can be performed using sensor channels located in bands (or on lines) of the water vapor absorption spectrum. The AVIRIS sensor has been used to retrieve water vapor (Green et al., 1989) and, with less accuracy, oxygen (Green et al., 1995a), carbon dioxide (De Jong et al., 1996), and ozone (Schl pfer et al., 1996a).

The influence of an atmospheric gas of interest on the radiance at the sensor level is usually simulated by radiative transfer codes. In this study, the spectral transmittance and the atmospherically scattered radiance are calculated by MODTRAN simulations with the Discrete Ordinates Radiative Transfer (DISORT) multiple scattering option (Kneisys et al., 1995). In the following sections the derivation and the implementation of the Atmospheric Precorrected Differential Absorption (APDA) technique is given.

<sup>\*</sup> Department of Geography, RSL, University of Z rich, Z rich, Switzerland

<sup>†</sup> Los Alamos National Laboratory, Los Alamos, New Mexico

<sup>‡</sup> Paul Scherrer Institut (PSI), Villigen PSI, Switzerland

Address correspondence to D. Schl pfer, Dept. of Geography, Remote Sensing Lab., Univ. of Z rich, CH-8057 Z rich, Switzerland. E-mail: dschlappf@geo.unizh.ch

Received 10 April 1996; revised 31 March 1998.

## COMPILATION OF DIFFERENTIAL ABSORPTION TECHNIQUES

Differential absorption techniques are a practicable way to determine gas contents from a spectrum of an absorption band at low computing time costs. They perform in general a ratioing between the radiance at channels within the absorption feature (measurement channels) and an interpolated radiance of channels in its vicinity (reference channels) to detect the relative strength of the absorption. This signal is related to the total column water vapor. Two major differential absorption techniques were used for hyperspectral imaging spectroscopy and compared by Carrère and Conel (1993): The Narrow/Wide technique (N/W; Frouin et al., 1990) and the Continuum Interpolated Band Ratio (CIBR; Green et al., 1989; Bruegge et al., 1990; Kaufman and Gao, 1992). A variation of the CIBR, the Linear Interpolated Regression Ratio (LIRR) was introduced by Schläpfer et al. (1996a). Table 1 shows a summarizing compilation of the three mentioned techniques. Curve fitting procedures (Gao

and Goetz, 1990a) are not considered in this study, primarily because of their higher computing time.

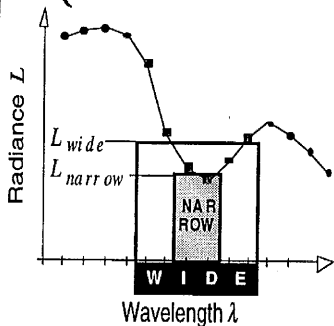
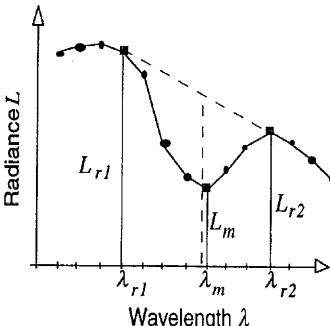
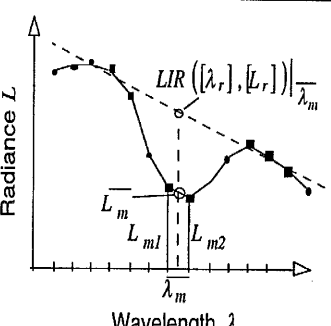
## DERIVATION OF THE ATMOSPHERIC PRE-CORRECTED DIFFERENTIAL ABSORPTION TECHNIQUE (APDA)

The radiance  $L$  measured in one specific channel by a sensor can be expressed as (Middleton, 1952):

$$L = \rho \frac{1}{\pi} E_0 T_{tot} + L_{atm}, \quad (1)$$

where  $E_0$  is the extraterrestrial solar irradiance and  $T_{tot}$  is the effective (observed) total transmittance of the Earth's atmosphere from the Sun to the ground and from the ground to the sensor. The apparent ground reflectance  $\rho$  includes the reflectance of the observed pixel as well as the path scattered radiance, reflected by the adjacent area (adjacency effect). In real data it therefore never will get to zero. The second term ( $L_{atm}$ ) is the backscattered atmospheric path radiance not reflected by the

Table 1. Summarizing of Differential Absorption Techniques Used for Water Vapor Retrieval

Technique:	Narrow Wide	Continuum Interpolated Band Ratio	Linear Regression Ratio
Acronym:	N/W	CIBR	LIRR
Figure :			
Equation:	$R_{N/W} = \frac{L_{narrow}}{L_{wide}}$	$R_{CIBR} = \frac{L_m}{\omega_{r1} \cdot L_{r1} + \omega_{r2} \cdot L_{r2}}$	$R_{LIRR} = \frac{\bar{L}_m}{LIR([\lambda_r], [L_r]) _{\lambda_m}}$
Parameters:	$L_{narrow}$ : (averaged) radiance in a narrow measurement band $L_{wide}$ : (averaged) radiance in a wide band at the same central wavelength as $L_{narrow}$	$\omega_{r1} = \frac{\lambda_{r2} - \lambda_m}{\lambda_{r2} - \lambda_{r1}}$ $\omega_{r2} = \frac{\lambda_{r1} - \lambda_m}{\lambda_{r2} - \lambda_{r1}}$	$\bar{L}_m$ : mean radiance of all measurement channels; $LIR([x], [y])$ : linear regr. line through points (x,y)
#Ref.-ch:	1 (includes measurement area)	2	at least 3
#Meas.-ch:	1	1	at least 1
Source:	Frouin, 1989	Bruegge, 1990	Schläpfer, 1996a
remarks	multispectral approach, in the hyperspectral case the channel sets are averaged	often used water vapor retrieval technique of high computational speed	extended CIBR technique, reduces total noise of the sensor

ground. All parameters of Eq. (1) depend on the wavelength of the used channel. The total transmittance is now split into the water vapor transmittance  $T_{wv}$  and a residual transmittance  $T_0$ , which depends on aerosol and gas absorption. The radiance at the sensor level  $L$  can then be expressed in a simple form as

$$L = \rho \frac{1}{\pi} E_0 T_0 T_{wv} + L_{atm} = L_{gnd} T_{wv} + L_{atm}, \quad (2)$$

where  $L_{gnd} = \rho \frac{1}{\pi} E_0 T_0$  is the total ground reflected radiance at the sensor level, if no water vapor were present.  $L_{atm}$  does not depend on the ground reflectance  $\rho$  but is sensitive to the atmospheric composition, in particular to the aerosol amount and the water vapor content.

Using this equation, we first write the radiances in three channels  $i=m, r1$  and  $r2$ , where  $m$  is a measurement channel in an absorption region, for example, the 940 nm water vapor absorption, and  $r1$  and  $r2$  are two reference channels on both sides of the absorption band. The transmittance  $T_{wv,m}$  is a function of water vapor for channel  $m$  but not for the reference channels  $r1$  and  $r2$  (i.e.,  $T_{wv,r1}=1$  and  $T_{wv,r2}=1$ ). Assuming a spectrally linear background reflectance in the range of the wavelengths  $\lambda_i$ , the radiance  $L_m$  in the measurement channel can be approximated by a linear interpolation as

$$L_m = [w_{r1} L_{gnd,r1} + w_{r2} L_{gnd,r2}] T_{wv,m}(PW) + L_{atm,m}(PW), \quad (3)$$

where [Eq. (4)]

$$o_{r1} = \frac{\lambda_{r2} - \lambda_m}{\lambda_{r2} - \lambda_{r1}} \quad \text{and} \quad w_{r2} = \frac{\lambda_m - \lambda_{r1}}{\lambda_{r2} - \lambda_{r1}}. \quad (4)$$

Solving Eq. (3) for the transmittance in the water vapor channel  $T_{wv,m}$  and substituting  $L_{gnd,r1}$  and  $L_{gnd,r2}$  from Eq. (2), we find an equation similar to the CIBR (see Table 1) but with precorrection terms for the atmospheric path radiances  $L_{atm,i}$ :

$$T_{wv,m} = \frac{L_m - L_{atm,m}(PW)}{w_{r1}(L_{r1} - L_{atm,r1}) + w_{r2}(L_{r2} - L_{atm,r2})}. \quad (5)$$

The atmospheric precorrection term  $L_{atm,i}$  is a function of terrain height, aerosol profile and contents, channel position, and water vapor contents. It can be estimated by calculating the total radiance at the sensor at zero albedo under varying ground altitude and water vapor contents [for a given aerosol optical depth, which has to be known approximately; see the text near Eq. (17) for details]. To increase the accuracy, an iterative approach is necessary. First, the path radiance is estimated based on the most probable water vapor contents. Then, the first water vapor result is taken as a second guess to calculate the improved path radiance estimate. In this derivation only one measurement and two reference channels are used. However, Eq. (5) can also be extended to more channels, analogous to the linear regression ratio, given in Table 1. The radiance values  $L$  of each channel

are reduced by the corresponding atmospheric path radiance terms  $L_{atm}$  and inserted in the LIRR equation. This equation is the common APDA equation which reduces directly to Eq. (5) for the three-channel case:

$$R_{APDA} = \frac{[L_m - L_{atm,m}]_i}{LIR([\lambda_r]_j, [L_r - L_{atm,r,j}] | [\lambda_m])}. \quad (6)$$

where  $LIR([x],[y])_a$  denotes a linear regression line through the points  $(x, y)$  evaluated for  $y$  at the point  $x=a$ . The parameters in brackets are the center wavelengths and atmospheric precorrected radiances of  $i$  measurement channels and  $j$  reference channels, respectively.

## COMPARISON OF THE APDA AND THE CIBR TECHNIQUE

### The CIBR Technique over Variable Background Albedos

The original CIBR technique uses the simulated radiance at the top of the atmosphere for the comparison with the measured radiance. Thus, atmospheric scattering effects are considered, but the influence of the atmospheric radiance on the ratio is neglected. At low ground reflectance, the atmospheric radiance is the major contributor to the total radiance, whereas at higher reflectance the ground reflected radiance term dominates. We introduce the total radiance following Eq. (2) into the CIBR equation (see Table 1). In the limit  $\rho \rightarrow 0$  the equation reduces to Eq. (7):

$$R_{CIBR}(\rho \rightarrow 0) \approx \frac{L_{atm,m}(PW)}{w_{r1} L_{atm,r1} + w_{r2} L_{atm,r2}}. \quad (7)$$

Since  $L_{atm,r1}$  and  $L_{atm,r2}$  are almost independent on the water vapor contents, the CIBR is then proportional to the water vapor-dependent atmospheric path radiance  $L_{atm,m}(PW)$ . When the background reflectance is high, the CIBR equation reduces to Eq. (8):

$$R_{CIBR}(\rho \rightarrow 1) \approx \text{const } T_{wv,m}. \quad (8)$$

Thus the CIBR is proportional to  $T_{wv,m}(PW)$  only for high background reflectances. At low background reflectances the water vapor retrieval gets less accurate, resulting in an underestimation over dark surfaces (Gao and Goetz, 1990a). The analogous calculations for the N/W technique lead to the same conclusions. This error could be corrected using a differential absorption procedure, which depends on the apparent reflectance at the sensor level. The presented APDA technique should correct for this effect based on the physical derivation given in the previous section.

### Evaluation over Simulated Reflectance Spectra at a Fixed Water Vapor Amount

The APDA equation (5) and the CIBR (see Table 1) were tested on MODTRAN-simulated radiance data. The at-

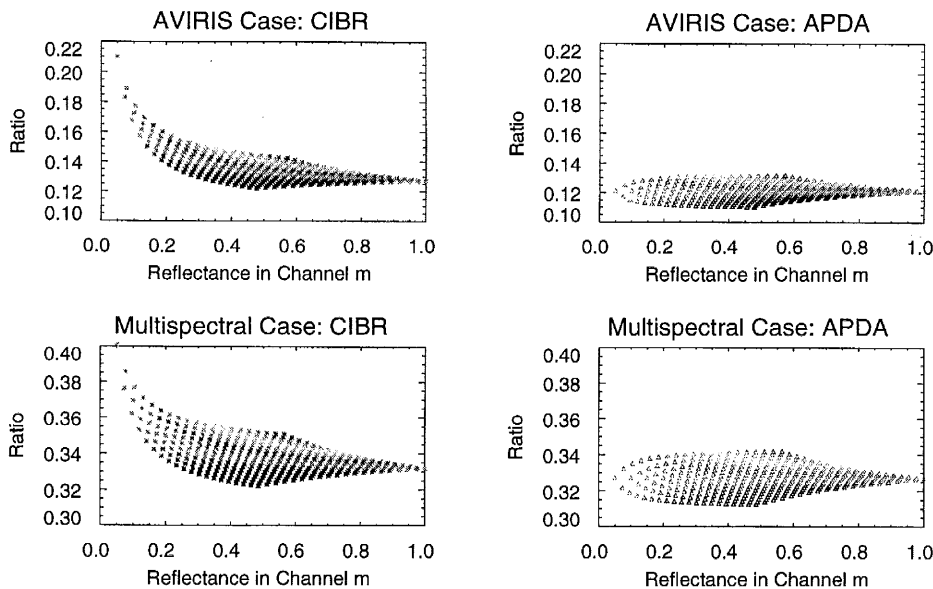


Figure 1. CIBR and APDA ratios for water vapor as a function of band-averaged ground reflectance of channel  $m$ . A 10 nm bandwidth instrument (AVIRIS) and a multispectral instrument (e.g., MODIS) are compared at constant water vapor amount.

mospheric state was midlatitude summer, the visibility at 23 km, and the columnar water vapor was fixed at 2.4 g/cm<sup>2</sup>. The target height was at 0.4 km, the Sun zenith angle at 40°, and the spectral resolution was set to 1 nm. The ground reflectances  $\rho_{r1}$  and  $\rho_{r2}$  were changed from 0.05 to 1.0 in steps of 0.05 on both sides of the spectral range ( $\lambda_{min(r1)}$ ,  $\lambda_{max(r2)}$ ), which is defined as the minimum and maximum wavelengths of Channels  $r1$  and  $r2$ , respectively. The following formula [Eq. (9)] is used to create the various reflectance background spectra:

$$\rho(\lambda) = \rho_{r1} + (\rho_{r2} - \rho_{r1}) \frac{\lambda - \lambda_{min(r1)}}{\lambda_{max(r2)} - \lambda_{min(r1)}}. \quad (9)$$

The selected AVIRIS bands (55, 62, and 68) for 1995 data have the following spectral range at full-width-half-maximum  $r1$ : 0.869–0.879  $\mu\text{m}$ ,  $m$ : 0.936–0.946  $\mu\text{m}$ , and  $r2$ : 0.994–1.004  $\mu\text{m}$  (see the next main section).

Figure 1 shows a scatterplot of all computed CIBR and APDA ratios as a function of the band-averaged reflectance in Channel  $m$ . The CIBR maps low reflectances ( $\rho_m < 0.2$ ) to higher ratios, thus lower water vapor. The APDA in contrast maps all reflectances to an almost constant ratio. The residual distribution of the ratio numbers originates from the varying reflectance slopes. This effect is similar for the CIBR and the APDA. Using broader bands, for example, in a future multispectral sensor such as MODIS, similar results are achieved. The selected bands have the spectral ranges  $r1$ : 0.86–0.89  $\mu\text{m}$ ,  $m$ : 0.91–0.97  $\mu\text{m}$ , and  $r2$ : 0.99–1.04  $\mu\text{m}$ . The ratios or quasi water vapor transmittances for the AVIRIS case are much lower than for the multispectral case because the narrower AVIRIS measurement channel has a more significant transmittance in the water vapor absorption feature.

### Evaluation over 379 Reflectance Spectra at a Variable Water Vapor Amount

The behavior of CIBR and APDA techniques over spectrally varying background was tested by another simulation. Existing reflectance spectral databases for 165 (Grove et al., 1991) and 25 (Kruse, 1992) minerals and 64 other spectra of natural and man-made materials were used as background. Since leaves contain significant amounts of water, a database for 125 simulated leaf reflectance and transmittance spectra with variable leaf water content (0.0046–0.0405 cm) was created using the PROSPECT model (Jacquemoud and Baret, 1990). The radiosity method (Borel et al., 1991) was then used to compute canopy spectra of a 20-layer canopy with a total leaf index (LAI) of 5.

All 379 reflectance spectra were resampled at 2.5 nm spacings. The radiative transfer code 6S (Vermote et al., 1994) was used to compute the top of atmosphere (TOA) radiance over the water vapor band centered on 940 nm. The water vapor amounts ranged from 1 g/cm<sup>2</sup> to 5 g/cm<sup>2</sup> in 12 steps. The atmosphere had a visibility of 20 km with continental aerosols. The target height was set at sea level and the sensor located above the atmosphere.

The original CIBR technique (see Table 1) and three variations of the APDA technique are compared. The three variations are:

APDA: The regular APDA equation (5) using a fixed water vapor amount of 3 g/cm<sup>2</sup> (out of 1–4 g/cm<sup>2</sup> range) to compute the water vapor dependent atmospheric path radiance  $L_{atm,m}(PW)$ .

APDA (optimal): Eq. (5) with known  $L_{atm,m}(PW)$ .

APDA (iterative): Eq. (5) with the iterative scheme described in the main section after next.

Table 2. Water Vapor Signal in Comparison to the Variation for Four Water Vapor Retrieval Techniques over 379 Background Spectra, Expressed as a Quasi-“SNR” Number<sup>a</sup>

Retrieval Technique	Case					
	AVIRIS			Multispectral		
	Range of R	SNR <sub>min</sub>	SNR <sub>max</sub>	Range of R	SNR <sub>min</sub>	SNR <sub>max</sub>
CIBR	0.243	14.7	15.8	0.267	16.7	17.9
APDA	0.253	21.5	58.7	0.277	18.4	42.1
APDA (optimal)	0.245	30.5	66.8	0.267	20.7	50.2
APDA (iterative)	0.246	30.5	66.6	0.270	21.2	49.7

<sup>a</sup> R and  $\sigma(R)$  are unit free ratio numbers.

The four techniques are compared by a measure similar to a quasi signal-to-noise ratio (SNR), which is based on the channel ratio number  $R$ , shown in Eq. (10):

$$SNR(R(PW)) = \frac{\bar{R}(PW_{min}) - \bar{R}(PW_{max})}{\sigma(R(PW))}, \quad (10)$$

where  $PW_{min} = 1 \text{ g/cm}^2$  and  $PW_{max} = 5 \text{ g/cm}^2$  are the minimum and maximum water vapor contents,  $\bar{R}(PW)$  denotes the average over  $R(PW)$ ,  $\sigma(R(PW))$  denotes the standard deviation of  $R(PW)$ . Table 2 shows the minimum and maximum SNR for the four retrieval techniques.

Next, we compare the retrieval methods by setting thresholds at  $\pm 5\%$  and  $\pm 10\%$  RMS relative water vapor and counting the number of spectra which indicates how robust the retrievals are over many different backgrounds. Table 3 summarizes the results obtained for all 379 background spectra using the four above described techniques. Figure 2 shows a scatterplot of the relative water vapor errors over 379 backgrounds as a function of band-averaged ground reflectance.

The CIBR underestimates the water vapor for low ground reflectance, where the regular and the iterative APDA work better. The AVIRIS case has fewer reflectance spectra outside the  $\pm 10\%$  limit than the multispectral approach, as is also evident from Table 3. In the scatterplots the simulated vegetation spectra show up as clustered sets of points along two lines between reflectances 0.55 and 0.66. The water vapor is overestimated because vegetation has a water absorption feature which increases the apparent water vapor in the atmosphere. This feature can be exploited to estimate canopy water content (Gao and Goetz, 1990b).

An analysis of the materials in which the iterative APDA had relative water vapor errors of more than

$\pm 10\%$  showed that nearly all of them were classified as spectrally sloped or nonlinear in the 940 nm band (Borel and Schl pfer, 1996). These special cases of background spectra still may lead to ground reflectance dependent errors in water vapor retrieval.

### Error Propagation Due to Sensor Noise

The measured radiances  $L_m$  and  $L_r$  are affected by the sensor noise. The noise is given by the noise equivalent radiance  $L_{ner}$  for each image channel (Green et al., 1996b). The APDA equation in general averages a number of measurement channels, what reduces the absolute error for  $n$  measurement channels to  $L_{err,m} = \sqrt{\sum (L_{ner,m}^2)/n}$ . The absolute error for the reference channels interpolation is described by the error of the linear regression intercept at the central channel position (Bevington and Robinson, 1992). The relative error of Eq. (6) is then calculated in relation to the ground reflected radiance at constant atmospheric conditions ( $PW = 2 \text{ g/cm}^2$ , rural aerosol type, visibility = 23 km). The relative noise uncertainty of the retrieved APDA ratios is below 3% for a ground reflectance above 10% (see Fig. 3). It increases to 4.5–5% reflectance with a further exponential increase towards zero reflectance. Thus, the method cannot be used for large black background targets, for example, for water. This effect is reduced over small dark targets, where the adjacency radiance contributes significantly to the total radiance at the sensor (note that only the radiance not reflected by the ground is subtracted in the APDA ratio). Atmospherically uncorrected ratios (CIBR/LIRR) are about half as sensitive to the image noise at low reflectances, where their systematic errors are high. An increasing number of measurement channels reduces the noise significantly, whereas additional reference chan-

Table 3. Percentage of Reflectance Spectra above 5% and 10% RMS Relative Water Vapor Derivation

Retrieval Technique	AVIRIS 5%	Multispectral 5%	AVIRIS 10%	Multispectral 10%
CIBR	35.36	32.98	9.50	13.19
APDA	8.18	21.11	1.85	3.17
APDA (optimal)	8.71	20.32	2.37	3.43
APDA (iterative)	7.92	20.32	1.85	3.17

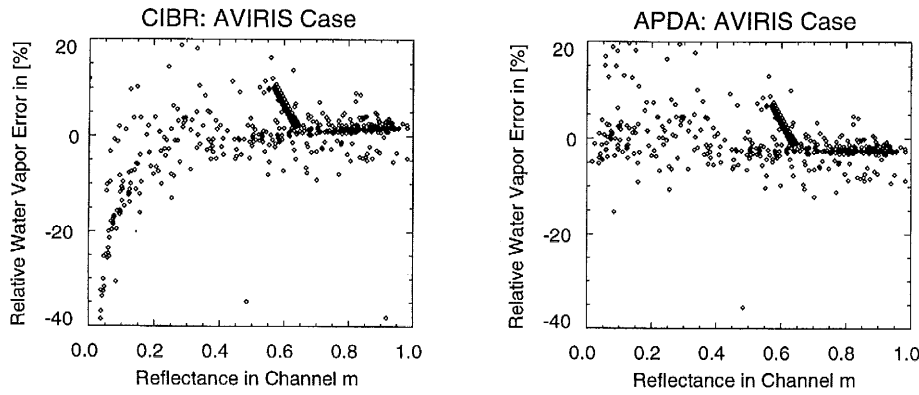


Figure 2. Relative water vapor errors over 379 backgrounds as a function of band-averaged ground reflectance for a 10 nm bandwidth instrument (AVIRIS). Note: The lined up points near 0.6 reflectance are from canopy spectra with simulated changing leaf water.

nels have only a minor impact on the error. The influence of the channel selection and variations in visibility are shown in the section after next.

## CHANNEL SELECTION

Both reference and measurement channels (see second section) are evaluated using the channel selection procedure proposed by Schlöpfer et al. (1995; 1996a). This methodology is the base to the APDA technique, considering the whole spectral range of one or more absorption features and picking the best channels based on the atmospheric state of a specific scene. The approach helps to avoid the use of erroneous channels while keeping the maximal amount of information on the investigated matter.

### Selection of Reference Channels

The signal of a reference channel should not be influenced by any atmospheric species and the effective signal to uncertainty ratio must be as large as possible. Thus, the channel selection indicator for the reference channels is defined as the product of an atmospheric transmittance factor  $M_{trans}$  and a radiance uncertainty fac-

tor  $M_{noise}$ . Introducing the expressions for the two factors yields the equation for the selection of reference channels (Schlöpfer et al., 1995; 1996a):

$$M_{ref} = M_{trans} \quad M_{noise} = [T_{wv} \quad T_0] \left[ \frac{L - \Delta L}{L} \right], \quad (11)$$

where

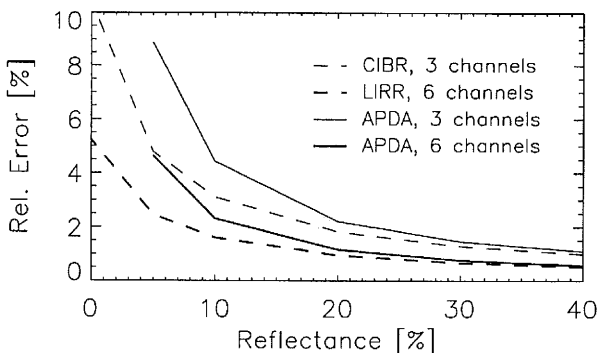
$$\Delta L = \sqrt{(L_{ner})^2 + (L_{scal})^2 + \left( \frac{\Delta \rho}{\rho} L_{gnd} \right)^2}. \quad (12)$$

The following parameters are simulated for each AVIRIS channel using the MODTRAN3 radiative transfer code: the apparent water vapor transmittance  $T_{wv}$ , the apparent total atmospheric transmittance  $T_0$  of all the other absorbing atmospheric species, the radiance at the sensor level  $L$ , and the total ground reflected radiance  $L_{gnd}$ .  $\Delta L$  is the effective total radiance uncertainty observed at the sensor as described in Eq. (12). It depends on three major parameters: first the total noise equivalent radiance  $L_{ner}$  of the sensor channel, then the radiance error due to spectral calibration uncertainty  $L_{scal}$  (both  $L_{ner}$  and  $L_{scal}$  are derived from the sensor specifications). Third, the influence of the relative ground reflectance radiance variation ( $\Delta \rho / \rho$ ) on the ground reflected radiance  $L_{gnd}$  in a channel is considered. This third factor is derived from the mean standard deviation of each image channel radiance. In addition, the wavelength distance of the reference channels from their corresponding measurement channels has to be considered. It has to be minimized to reduce errors due to spectrally nonlinear background reflectance characteristics.

### Selection of Measurement Channels

Measurement channels are searched within the absorption band because they should be sensitive to variations of the water vapor (described by the sensitivity measure  $M_{sens}$ ). Furthermore, the difference between the signal of water vapor and the noise must be clearly discernible in these channels (significance,  $M_{sign}$ ) and other absorbing atmospheric species must not disturb the signal (cross sensitivity,  $M_{cross}$ ). The product of these three parameters leads to a common wavelength dependent selection equation for

Figure 3. Relative error of the APDA and the CIBR technique due to sensor noise propagation in relation to the ground reflectance. The six channel ratios combine two measurement channels and four reference channels.



measurement channels (Schläpfer et al., 1995; 1996a):

$$M_{meas} = M_{sens} \quad M_{sign} \quad M_{cross} \\ = [-e \quad T_{wv} \quad \ln(T_{wv})] \left[ \frac{(L_0 - L) - \Delta L}{L_0 - L} \right] [T_0]. \quad (13)$$

The crucial factor of Eq. (13) is the sensitivity measure  $M_{sens} = \text{const} \cdot \partial T_{wv} / \partial PW = -e \quad T_{wv} \quad \ln(T_{wv})$ , presuming Beer-Lambert's law ( $T_{wv} = e^{-k \quad PW}$ ). It describes the relative change of the transmittance, based on a water vapor variation at a fixed average water vapor content  $PW$ . The normalizations constant (const) is taken such that  $\max(M_{sens}) = 1$ .  $M_{sens}$  is maximal for  $T_{wv} = 1/e$ . Lower transmittances tend to saturate, whereas at higher transmittance the signal of water vapor is too low. The encountered transmittance per image channel is dependent on the specific atmospheric conditions. Therefore, the selected measurement channels differ between situations with differing column water vapor contents. The measure ( $M_{sign}$ ) is dependent on the significance of the absorbed radiance ( $L_0 - L$ ) in the water vapor band compared to the effective total radiance uncertainty  $\Delta L$  [see Eq. (12)].  $L_0$  is the radiance at the sensor level if no water vapor would be present.  $M_{sign}$  becomes negative, when the total radiance uncertainty is greater than the observed absorption signal. Finally, the cross sensitivity measure  $M_{cross}$  is taken directly from the total atmospheric transmittance at a water vapor amount of zero ( $T_0$ ).

### Channel Selection Results for AVIRIS Data

The channel selection procedure was applied to MODTRAN-simulated data corresponding to AVIRIS images from 1991 over Central Switzerland and from 1995 over Camarillo (California). Ranked sets of channels to be used in the APDA technique were defined. A selection threshold was introduced on the measures  $M_{meas}$  and  $M_{ref}$ , to select a reduced set of five measurement and six reference channels, excluding the worst channels from further consideration. A first analysis showed that the best-suited water vapor absorption feature for nadir viewing sensors under intermediate atmospheric conditions ( $\approx 2$ –3 cm of precipitable water vapor) is the 940 nm band. Hence, only channels between about 850 nm and 1070 nm were further considered (see Table 4). At lower water vapor contents (below 1 cm), a stronger band with sufficient absorption may be considered, whereas at high contents the channels in the band slopes are favored.

A crucial factor for the measurement channel selection is the average total water vapor transmittance, which has to be estimated from total columnar water vapor content for each scene. It was integrated from radio-sonde profiles, taken at the overflight time. For operational use however, it can also be taken from standard atmospheric profiles. A plot of the single factors, following the Eqs. (13) and (11), for 1995 and 1991 AVIRIS channels is shown in Figure 4. Table 4 lists the selected channels for the two datasets.

### IMPLEMENTATION OF THE APDA TECHNIQUE

The differential absorption technique only yields ratio values (corresponding to a quasi gas transmittance), which need to be transformed to total water vapor amounts. Frouin et al. (1990) and Carrère et al. (1993) used an exponential approach to relate the differential absorption ratio  $R$  to the corresponding water vapor amount ( $PW$ ). For the present study this correlation was extended to an equation with three empirical regression parameters  $a$ ,  $\beta$ , and  $\gamma$ :

$$T_{wv}(PW) \approx R_{APDA} = e^{-(\gamma + a(PW)^\beta)}, \quad (14)$$

solved for the water vapor amount,

$$PW(R_{APDA}) = - \left( \frac{\ln(R_{APDA}) + \gamma}{a} \right)^{1/\beta} \quad (15)$$

This equation fits the MODTRAN derived APDA results for the expected variation of the atmosphere in water vapor and aerosols and therefore is valid only for the investigated range of water vapor. It allows one to decrease the computing time for the look-up table inversion from nearly 1 h to less than 1 min, the potentially induced errors being less than 1%. The regression parameters are retrieved only once at the beginning of the calculation as best fit to all simulated atmospheric situations. The values for  $a$  range from 0.12 to 0.18, for  $\beta$  from 0.65 to 0.80, and for  $\gamma$  from  $-0.05$  to  $0.4$ , depending on the absolute water vapor amount, the range of the water vapor amounts, the aerosol contents, and the assumptions on background reflectance characteristics.

The following iterative procedure is used to compute the water vapor image (compare Fig. 5 for a flow chart of the overall APDA procedure):

1. Use a radiative transfer code to compute a look-up table (LUT) containing the total

Table 4. Selected AVIRIS Channels for 1991 and 1995 Data Sets

Channels:	AVIRIS 1991	AVIRIS 1995
Measurement	57, 59–62 (910, 930–959 nm)	61–64 (932–961 nm)
Reference	52–54 (862–881 nm)	54–56 (865–884 nm)
(near the selected meas. channels)	66–70 (987–1036 nm)	68–70 (999–1018 nm)

amounts using the function in Eq. (14) and store the fitting parameters  $\alpha$ ,  $\beta$ , and  $\gamma$ .

4. Assume a starting water vapor content ( $PW_1$ ) for all image pixels and subtract the height-dependent path radiance term from the image.
5. Calculate the APDA ratio following Eq. (6) and transform the ratio values to water vapor contents ( $PW_2$ ), using Eq. (15).
6. Substitute the values of  $L_{atm}$  in Eq. (6) with the new water-vapor-dependent values, derived from the LUT.
7. Calculate the image ratio  $R_{APDA}$  a second time and transform the ratio values to the final water vapor contents  $PW_3(x,y)$ .

Steps 5 and 6 could be repeated, but our computations have shown that these two iterations converge sufficiently.

## IMAGE BASED OPTIMIZATION OF THE APDA TECHNIQUE

### Error Analysis for Varying Channel Combinations and Aerosol Contents

In the following, the term “method” is used for a APDA ratio based on one specific channel combination set; 270 methods were investigated for the 1991 data and 108 methods for 1995 based on the preselected channels. A spatial test image subset is interactively defined as an adjacent region of the image, where ground reflectance variations are high and terrain influence is low (e.g., flat agricultural fields). A good method for the measurement of a particular gas must show little sensitivity to noise, background, and aerosol variations. An indicator for the noise and background effect is found based on the standard deviation  $\sigma(PW_{sub})$  of the water vapor retrieval results within the subset. It is assumed that the effective water vapor variation  $\sigma(PW_{wv,sub})$  and the uncertainty signal  $\sigma(PW_{\Delta L,sub})$  overlay each other independently. Therefore, the standard deviation of the water vapor content over the subset and for each considered method is taken as indicator value, which should be minimal, as shown in Eq. (16):

$$\sigma(PW_{sub}) \rightarrow MIN, \quad \text{where} \quad \sigma(PW_{sub}) = \sqrt{\sigma^2(PW_{wv,sub}) + \sigma^2(PW_{\Delta L,sub})}. \quad (16)$$

The effects of the measurement channel position for 1991 and 1995 data are shown in Figure 6. In both data sets the measurement channels around 930 nm tend to an underestimation of about 10%, which probably is related to the position of these bands in the steeply falling water vapor transmittance at this wavelength. At larger wavelengths (channels 62 and 64), a higher water vapor content is estimated. This pattern can come either from the increased liquid leaf water absorption at this wavelength or from an unknown spectral channel position shift.

The  $PW$  estimates over the subsets of both datasets for different reference channel combinations (at constant

measurement channels) are found to be within insignificant  $\pm 2\%$ . An increasing number of reference channels has an only marginal influence on the retrieval results. Therefore, only methods with up to four reference channels have to be considered. The APDA (60,61;54,67) method (notation: APDA ( $m_i, r_j$ )) was finally selected for application to the images of 1991 and the ADPA (61,62; 54,55,68,69) for 1995 data. The relative standard deviation [ $\sigma(PW_{sub}) \cdot 100 / \text{mean}(PW_{sub})$ ; “image noise”] over the image subset was at 2.5% in 1991 and at 2% in 1995 [down to  $\sigma(PW_{sub}) = 0.04$  cm]. This difference of the image subset standard deviation is dependent on the significantly improved SNR values of the AVIRIS data in 1995.

The influence of aerosols is determined using MODTRAN3 simulations with constant water vapor amount but changing aerosol amounts (by varying the visibility stepwise from 10 km to 40 km at ground level). The standard deviation of the corresponding derived water vapor amounts [ $\sigma(PW_{vis}) \rightarrow MIN$ ] is taken as a second indicator for the method selection. The resulting RMS error is nearly twice as large for methods with measurement channels in the slope of the band ( $\pm 3$ –6%) than for those in the center ( $\pm 1.5$ –3%) (see Fig. 6). For both selected methods the estimated RMS errors due to the simulated aerosol variation was below 0.09 cm (PW), which is a relative error of 2–3%.

### Statistical Retrieval of the Atmospheric Path Radiance Term

The atmospheric path radiance term  $L_{atm}$  in the APDA equation (6) is dependent on the aerosol and water vapor distribution as a function of terrain elevation. Initially, the aerosol content is defined using a standard model at estimated visibility. An adjusted atmospheric path radiance  $L_{atm,i}$  term is found empirically to be

$$L_{atm,i} = L_{atm,i}^M \left( 1 + a \frac{g_i}{g_{max}} \right), \quad \text{where} \quad g_i = \frac{L_{atm,i,max}^M - L_{atm,i,min}^M}{L_{atm,i,min}^M}, \quad (17)$$

where  $a$  is an empirical adjustment parameter and  $L_{atm,i}^M$  is the basic first assumption for the amount of atmospheric path radiance, as derived from MODTRAN for channel  $i$ . The weighing factor  $g_i$  describes how strongly the state of the atmosphere influences the atmospheric path radiance term in each channel. It is found from the ratio between a maximum and a minimum atmospheric path radiance: The value  $L_{atm,i,max}^M$  is taken at dry atmosphere with high aerosol concentrations (lowest altitude in the LUT), in direct contrast to  $L_{atm,i,min}^M$  (highest altitude and humid atmosphere). The weighing factor  $g_i$  is normalized by the maximal weighing factor  $g_{max}$  of all channels within the LUT.

The channel independent parameter  $a$  is only valid for one specific method applied to the investigated image scene. It is derived by minimizing the standard deviation



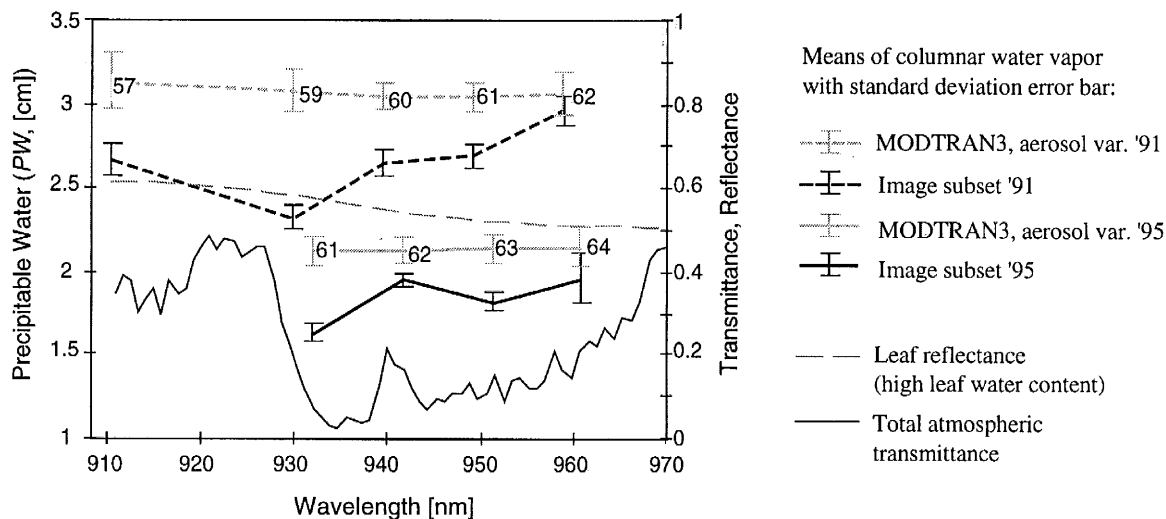


Figure 6. Qualification results for APDA techniques with one measurement channel for 1991 and 1995 data and for simulated atmospheric conditions. The obvious underestimation in the channels 59 (1991) and 61 (1995), respectively, and their higher variation due to aerosol loading may origin from the steep total transmittance slope. The leaf water reflectance on the other hand may influence channels 62 and 64, respectively.

$\sigma(PW_{sub})$  over the image subset (as described in the previous subsection) while adjusting the path radiance term with Eq. (17). The obtained values for  $a$  in the investigated scenes were  $-0.10$  and  $-0.18$ , respectively. This indicates, that the initial assumptions on atmospheric path radiance were correct within an error range of about 20%.

#### APPLICATION OF THE APDA TECHNIQUE TO AVIRIS DATA

The methodology described in the previous sections was applied to two AVIRIS scenes (Schlöpfer et al. 1996b):

1. Site: Central Switzerland, "Risch" Date: 5 July 1991 (AVIRIS 070591 run 6, scene 1).
2. Site: Santa Monica, "Camarillo" Date: 26 May 1995 (AVIRIS 052695 run 8, scene 3).

##### Central Switzerland

The selected differential absorption method for 1991 was applied to the AVIRIS '91 scene of Central Switzerland (Meyer, 1994). The SNR of the 1991 data was only one fifth compared to the most recent AVIRIS data. However, this data set is valuable for atmospheric imaging spectroscopy because of the extensive simultaneous *in situ* measurements of atmospheric trace gases. Various soundings in and near the test region were combined to obtain the actual profile for the date of over flight.

The AVIRIS scan was georectified at high accuracy by Meyer (1994). The fully height-dependent APDA technique could therefore be applied to this mountainous scene. The water vapor retrieval results of the APDA (60,61;54,67) method are shown in Figure 7. The mean

column water vapor along the shore of the lake as measured from the image is about 2.85 cm. The integration of the *in situ* water vapor profiles yields a total column of 2.97 cm over the lake level (414 m a.s.l.). This small difference of about 5% between radiosonde data and the AVIRIS-retrieved column water vapor is within the error of radiosonde data in general (about  $\pm 10\%$  for column water vapor) and also within the error range of the retrieval procedure described above. An even better agreement is found when comparing the retrieval difference between the highest and the lowest terrain pixels to the corresponding integrated radiosonde profile.

The meteorological interpretation of the water vapor distribution in rugged terrain using the calculated images is difficult because the influence of the terrain overrides real horizontal changes in water vapor concentrations. To reduce this terrain effect, the procedure described in Schlöpfer et al. (1997) is used. The resulting terrain adjusted water vapor retrieval for LIRR and APDA calculation is shown in Figure 7. In the uncorrected image, obvious underestimations over the relatively dark forests can be observed. If the atmospheric precorrection is applied, a significant improvement is achieved. Most of the errors caused by variations of the background reflectance disappear, leading to a better estimate of relative water vapor concentrations. In the not adjusted distribution images the influence of the terrain overrides such background effects.

##### Scene over Camarillo, California

The application of the APDA technique on the 1995 data showed the unexpected effects of edge enhancement

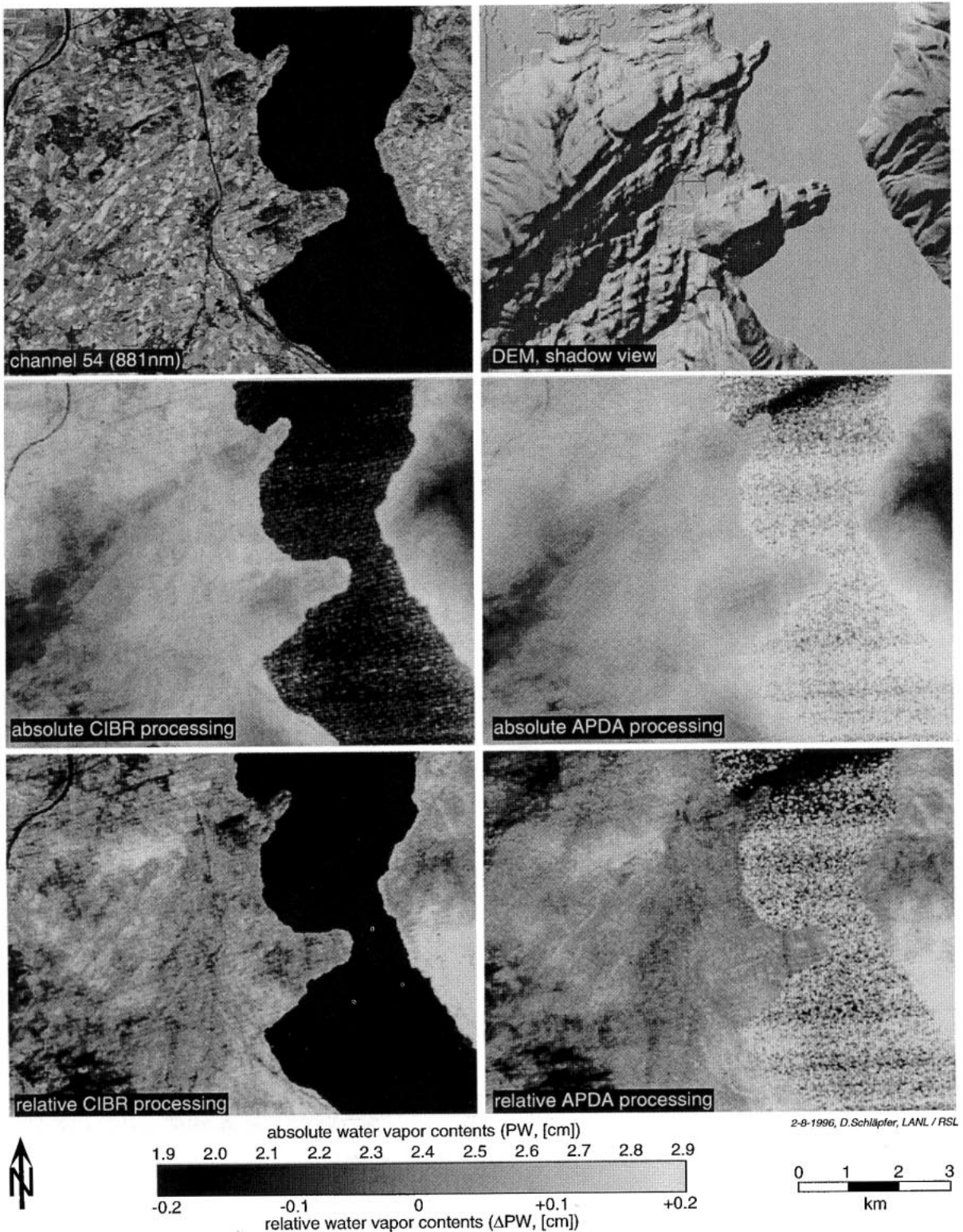


Figure 7. Processing of 1991 AVIRIS data, Central Switzerland, using channels 54, 60, 61, and 67. Upper Images: Near-infrared channel 54 (left) and DEM used for the geocoding of the image (right). Middle images: Absolute water-vapor retrieval with CIBR (left) and APDA technique (right). Lower images: Relative water vapor distribution ( $\Delta PW$ ) resulting from CIBR (left) and APDA (right).

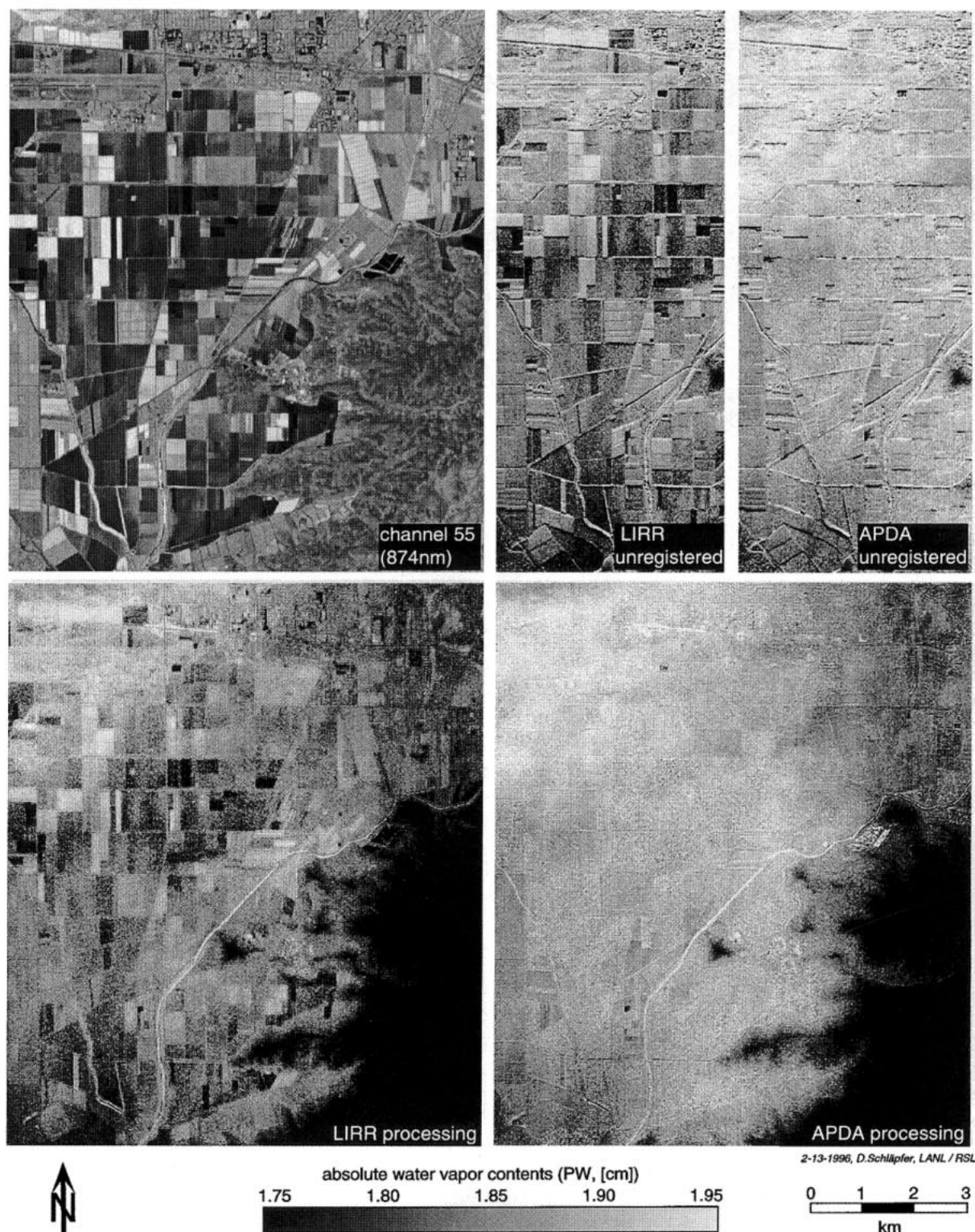


Figure 8. Processing of 1995 AVIRIS data, Camarillo, using channels 54, 55, 61, 62, 68, and 69. Upper left: raw channel 54, upper right: unregistered LIRR resp. APDA processing (no pixel shifting applied). Lower left: LIRR (=CIBR) processing (after pixel shift registration), Lower right: APDA processing.

along the borders of the agricultural fields (see Fig. 8 upper right images). Since cast shadows in irrigation channels and from plants would not show this phenomenon in a systematic way, a sensor inherent effect is supposed. According to Chrien (personal communication, 1996), the new AVIRIS focal plane is equipped with slower slew rate amplifiers which cause bright areas bounded by dark areas to appear somewhat delayed. The delay increases with the magnitude of changing signal. Since the reference channels have more than twice the signal of the measurement channels, their delay was significantly higher. To correct for this effect, we introduced a spatial shift between single channels. A procedure to detect subpixel shifts (Varosi, 1988–1995) was applied for the channels used in the water vapor retrieval algorithm. This analysis, which maximizes the correlation between the single channels, showed that the reference channels (54, 55, 56, 68, 69, and 70) were shifted in scan direction by about 0.15 pixels with respect to the measurement channels (60, 61, 62, and 63). In flight direction nearly no shift was detected. All relevant channels were then registered by the calculated subpixel shifts, using bilinear interpolation. The corrected water vapor images (lower images in Fig. 8) were significantly improved compared to the unregistered images.

Furthermore, Figure 8 shows the effects of the atmospheric precorrection: When performing the traditional differential absorption technique, high impacts of the background characteristics are reported, with underestimations over dark surfaces (lower left image). After the atmospheric precorrection, most of this impact disappears (lower right image). The resulting water vapor distribution is much less biased by the land use features than the previous water vapor calculation (the smoother appearance is not a filtering effect but is only due to the applied correction!). The range of water vapor is within about 1.7–2.0 cm, and even fine variations over the plane between 1.8 cm and 1.9 cm can be observed in the shift corrected APDA image. A radiosonde profile from the date of data acquisition reports an amount of 2.05 cm above sea level. The difference of 5–10% is within radiosounding accuracy and can also origin from water vapor variations during daytime. In the final image there are some remaining small ground reflectance caused effects, which show that there is still an opportunity to improve the water vapor retrieval.

## CONCLUSIONS AND OUTLOOK

An efficient technique to determine the amount of columnar water vapor has been derived from a modified radiative transfer equation. We simulated the behavior of the original CIBR and the APDA over dark, bright, and spectrally variable backgrounds. Additionally, a large number of spectra from minerals, man-made surfaces, and vegetation canopies was used. The relative water vapor error lies

within  $\pm 5\%$  for most of these ground reflectance spectra. Ranked sets of channels were selected quantitatively prior to the application of the APDA technique to a specific scene. The sophisticated channel selection procedure allows to define ideal channel positions and combination for any hypothetical or real scene.

We showed that the new atmospheric precorrected differential absorption (APDA) technique allows the accurate measurement of spatial water vapor distributions even over flat areas with strong background reflectance variations. Note that we have not yet investigated completely how the APDA technique depends on aerosol stratification, sensor calibration errors, and radiative transfer code uncertainties. Nevertheless, the accuracy is sufficient for current applications, since these additional sources are estimated to cause similar small relative errors. The presented techniques may also be useful to retrieve other gases with absorption features in the visible or near-infrared part of the spectrum, such as  $O_2$  or  $O_3$ .

The basic APDA technique is fully automatized and performs in less than 1 min for an AVIRIS scene (if the look-up table is already created). Further automatization could be achieved by using a set of MODTRAN standard look-up tables together with predefined channel combinations. Second, an average aerosol loading could be estimated with the described procedure, by using the DEM and statistical information of the image to define a suited image subset automatically. The distribution of the water vapor with terrain height for 1991 data was very similar to the profile measured by radiosondes. Hence, the resulting APDA-images can be used to derive water vapor profiles from the boundary layer along terrain slopes. Note that accurate geocoding of the images on top of digital elevation models is necessary for such processing.

A challenge remains to retrieve the water vapor over dark surfaces such as water or shadowed areas, since the path radiance is there the only quantity containing information about the atmosphere. This complementary measurement of water vapor will only be possible with further improvements of the methodology. Such techniques may differ from differential absorption and nonlinear curve fitting techniques. The most promising approaches are the improvement of the atmospheric precorrection by considering adjacency effects and using the full amount of radiance at the sensor level for the retrieval technique.

---

*The following institutions, foundations, and persons are greatly acknowledged: The Swiss National Science Foundation, the Paul Scherrer Institute (Switzerland), NASA's Remote Sensing Science Programs and the U.S. Department of Energy for the financial support of the project, the AVIRIS group at the Jet Propulsion Laboratory (JPL) Pasadena, California, for providing the AVIRIS images, Los Alamos National Laboratory (LANL), and the Remote Sensing Laboratories (RSL), Zürich, for their facilities. We acknowledge many fruitful technical discussions with and work done by Veronique Carrère (ISPR, Italy), James Theiler (LANL), and Bill Clodius (LANL).*

## REFERENCES

- Bevington, P. R., and Robinson, D. K. (1992), *Data Reduction and Error Analysis for the Physical Sciences*, McGraw-Hill, New York, 330 pp.
- Borel, C. C., and Schläpfer, D. (1996), Atmospheric pre-corrected differential absorption techniques to retrieve columnar water vapor: theory and simulations. In *6th Annual JPL Airborne Earth Science Workshop*, Jet Propulsion Laboratory, Pasadena, CA, pp. 13–21.
- Borel, C. C., Gerstl, S. A. W., and Powers, B. J. (1991), The radiosity method in optical remote sensing of structured 3-D surfaces. *Remote Sens. Environ.* 36:13–14.
- Bruegge, C. J., Conel, J. E., Margolis, J. S., et al. (1990), In-situ atmospheric water-vapor retrieval in support of AVIRIS validation. In *Imaging Spectroscopy of the Terrestrial Environment*, SPIE Vol. 1298, pp. 150–163.
- Carrère, V., and Conel, J. E. (1993), Recovery of atmospheric water vapor total column abundance from imaging spectrometer data around 940 nm—sensitivity analysis and application to Airborne Visible/Infrared Imaging Spectrometer (AVIRIS) Data. *Remote Sens. Environ.* 44:179–204.
- De Jong, S. M., and Chrien, T. G. (1996), Mapping volcanic gas emissions in the mammoth mountain area. In *6th Annual JPL Airborne Earth Science Workshop*, Jet Propulsion Laboratory, Pasadena, CA, pp. 75–80.
- Frouin, R., Deschamps, P.-Y., and Lecomte, P. (1990), Determination from space of atmospheric total water vapor amounts by differential absorption near 940 nm: theory and airborne verification. *J. Appl. Meteorol.* 29:448–459.
- Gao, B.-C., and Goetz, A. F. H. (1990a), Determination of total column water vapor in the atmosphere at high spatial resolution from AVIRIS data using spectral curve fitting and band ratioing techniques. In *Imaging Spectroscopy of the Terrestrial Environment*, SPIE Vol. 1298, pp. 138–149.
- Gao, B.-C., and Goetz, A. F. H. (1990b), Column atmospheric water vapor and vegetation liquid water retrieval from Airborne Imaging Spectrometer data. *J. Geophys. Res.* 95(D4): 3549–3564.
- Gao, B.-C., Heidebrecht, K. B., and Goetz, A. F. H. (1993), Derivation of scaled surface reflectance from AVIRIS data. *Remote Sens. Environ.* 44:165–178.
- Green, R. O., Carrère, V., and Conel, J. E. (1989), Measurement of atmospheric water vapor using the Airborne Visible/Infrared Imaging Spectrometer. In *Workshop Imaging Processing*, Sparks, Nevada, Am. Soc. Photogramm. and Remote Sensing, 6 pp.
- Green, R. O., Roberts, D. A., and Conel, J. E. (1996a), Characterization and compensation of the atmosphere for the inversion of AVIRIS calibrated radiance to apparent surface reflectance. In *6th Annual JPL Airborne Earth Science Workshop*, Jet Propulsion Laboratory, Pasadena, CA, pp. 136–146.
- Green, R. O., Conel, J. E., Margolis, J., Chovit, C., and Faust, J. (1996b), Calibration of the Airborne Visible/Infrared Imaging spectrometer in the laboratory. In *6th Annual JPL Airborne Earth Science Workshop*, Jet Propulsion Laboratory, Pasadena, CA, pp. 115–126.
- Grove, C. I., Hook, S. J., and Paylor, E. D. (1992), *Spectral Reflectance of Minerals 0.4 to 2.5 Micrometers*, JPL Publication 92-2, Jet Propulsion Laboratory, Pasadena, CA, 406 pp.
- Jacquemoud, S., and Baret, F. (1990), PROSPECT: a model of leaf optical properties spectra. *Remote Sens. Environ.* 34: 75–91.
- Kaufman, Y. J., and Gao, B.-C. (1992), Remote sensing of water vapor in the near IR from EOS/MODIS. *IEEE Trans. Geosci. Remote Sens.* 30(5):871–884.
- Kneisy, F. X., Abreu, L. W., Anderson, G. P., et al. (1995), *The MODTRAN 2/3 and LOWTRAN 7 Model*, Philips Laboratory, prepared by Ontar Corporation, North Andover, MA, 267 pp.
- Kramer, J. H. (1994), *Observation of the Earth and Its Environment, Survey of Missions and Sensors*, 2nd ed., Springer-Verlag, Berlin, pp. 169–186.
- Krishna Rao, P., Holme, S. J., Anderson, R. K., Winston, J. S., and Lehr, P. E. (1990), *Weather Satellites: Systems, Data, and Environmental Applications*, American Meteorological Society, Boston, Section III & IV, pp. 49–132.
- Kruse, F. A. (1992), unpublished data, IUGS Special Publication, Boulder CO.
- Meyer, P. (1994), A parametric approach for the geocoding of Airborne Visible/Infrared Spectrometer (AVIRIS) data in rugged terrain. *Remote Sens. Environ.* 49:118–130.
- Middleton, W. E. K. (1952), *Vision through the Atmosphere*, University of Toronto Press, Toronto.
- Schläpfer, D., Keller, J., and Itten, K. I. (1995), Imaging spectrometry of tropospheric ozone, New methods of channel selection, IGARSS'95, separatum, 3 pp. (available at: <http://www.geo.unizh.ch/dschlapf/paper.html>).
- Schläpfer, D., Keller, J., and Itten, K. I. (1996a), Imaging spectrometry of tropospheric ozone and water vapor. In *Proceedings of the 15th EARSeL Symposium Basel* (E. Parlow, Ed.), A. A. Balkema, Rotterdam, pp. 439–446 (available at: <http://www.geo.unizh.ch/dschlapf/paper.html>).
- Schläpfer, D., Borel, C. C., Keller, J., and Itten, K. (1996b), Atmospheric pre-corrected differential absorption techniques to retrieve columnar water vapor: application to AVIRIS 91/95 data. In *5th Annual JPL Airborne Earth Science Workshop*, Jet Propulsion Laboratory, Pasadena, CA, pp. 209–217.
- Schläpfer, D., Keller, J., and Itten, K. I. (1997), Retrieval of the horizontal and the vertical water vapor distribution from AVIRIS data. In *7th International ISPRS Symposium on Physical Signals in Remote Sensing*, Courchevel, France, pp. 591–598.
- Varosi, F. (1988–1995), *Varosi's General Purpose IDL Code Library* (vlib), Mail Code 685, <ftp://idlastro.gsfc.nasa.gov/c>, NASA/Goddard Space Flight Center, Greenbelt, MD.
- Vermote, E., Tanré, D., Deuzé, J. L., Herman, M., and Morcrette, J. J. (1994), *Second Simulation of the Satellite Signal in the Solar Spectrum*, 6S User Guide, NASA-Goddard Space Flight Center, Greenbelt, MD, 182 pp.